

Basal membrane complex architecture is disrupted during posterior subcapsular cataract formation in Royal College of Surgeons rats

Anita Joy,¹ Kristin J. Al-Ghoul^{2,3}

¹Department of Growth, Development and Structure, Southern Illinois University School of Dental Medicine, Alton, IL;

²Department of Anatomy and Cell Biology, Rush University Medical Center, Chicago, IL; ³Department of Ophthalmology, Rush University Medical Center, Chicago, IL

Purpose: Previous studies detailing the development of posterior subcapsular cataracts (PSC) in Royal College of Surgeons (RCS) rats have shown that aberrant fiber-end migration underlies the structural compromise. This investigation was conducted to examine the distribution of select basal membrane complex (BMC) components and to assess the intravitreal levels of specific cytokines during PSC formation.

Methods: Lenses from 52 RCS dystrophic rats (RCS/Lav) and 28 genetically matched control animals (RCS-rdy⁺/Lav) from 2 to 8 weeks old were used. After enucleation, vitreous was collected for eventual cytokine level analyses; lenses were then removed and processed for immunocytochemical localization of actin, cadherin, β integrin, vinculin, and cell nuclei.

Results: At 2–3 weeks postnatal, dystrophic lenses showed normal BMC distribution of actin, cadherin, and vinculin; however β integrin distribution was altered as compared to controls. By 4–6 weeks of age, F-actin was visible as bright foci arranged in a “rosette” pattern around fiber-end profiles. Concurrently, vinculin was rearranged into a diffuse pattern within the BMC. Cadherin delineated the fiber ends in dystrophic lenses until 5 weeks postnatal, after which it displayed diffuse cytoplasmic staining with more definitive labeling at the BMC periphery. β integrin was initially distributed as punctuate spots at 2–3 weeks postnatal; however, by 4–6 weeks it was co-localized with F-actin around the periphery of fiber ends. The distribution of F-actin, cadherin, and β integrin components did not undergo further changes after 6 weeks of age; however, vinculin was present predominantly at the periphery of the BMC in 7–8-week-old dystrophic lenses. Intravitreal cytokine levels were assessed for interleukin (IL)-1 α , IL-4, IL-6, IL-8, tumor necrosis factor (TNF), and interferon (IFN)- γ . Levels of IL-1 α , IL-4, TNF, and IFN- γ demonstrated a similar pattern, with concentrations increasing from 2 to 6 weeks postnatal and then decreasing slightly up to 8 weeks of age. IL-4 and TNF had the highest average concentrations, with peaks of 148.00 pg/ml and 34.20 pg/ml, respectively.

Conclusions: The data indicate that defined rearrangements of normal BMC architecture precede and characterize the structural changes that culminate in the PSC. These are consistent with modifications of adhesion mechanics involving cell–cell attachment, cell–matrix adhesion, and timely fiber-end detachment. Further, the results suggest that pro-inflammatory cytokines are potential initiating factors in aberrant fiber-end migration and subsequent PSC formation.

A critical process that occurs during lens fiber differentiation is the coordinated migration of elongating fiber ends along the epithelium (anteriorly) and the capsule (posteriorly). Fiber migration is a highly coordinated and regulated progression that involves adhesion, translocation, and detachment of fiber ends, and on the posterior aspect the entire process is mediated by the basal membrane complex (BMC). The BMC of avian lens fibers includes the basal domain of the fiber-cell membrane, the integral membrane proteins, and their associated cytoskeletal elements [1]. The BMC is an important area that includes molecules such as integrins, cadherins, actin,

myosin, and caldesmon. Several molecules of the BMC, such as actin, β -1 integrin, and N-cadherin, have been studied to show their role in cell attachment, migration, and proliferation during fiber differentiation.

Studies have definitively shown that β -1 integrins are the primary integrin receptor for the basal lamina proteins in the lens capsule [2]. The integrins act as bidirectional signaling receptors [3], mediating interactions between the cytoskeleton and extracellular matrix that affect proliferation, adhesion, and fiber-cell polarity [4–6]. N-cadherin, a cell adhesion molecule, has also been implicated in lens fiber differentiation. Through its linkage to actin, N-cadherin regulates differentiation-dependent cytoskeletal reorganization [7]. N-cadherin is co-localized with actin both within the native BMC and in cell culture [1,7–9]. In addition, actin has also been found to play an important role in coordinating

Correspondence to: Kristin J. Al-Ghoul, Department of Anatomy and Cell Biology, Rush University Medical Center, 600 S. Paulina St., Ste 507, Chicago, IL 60612; Phone: (312) 563-2672; FAX: (312) 942-5744 email: kristin_j_al-ghoul@rush.edu

structural changes and maintaining the integrity of lens development during fiber-cell elongation [1,10-15].

Although the BMC of rodent lenses consists of virtually the same components as avian lenses, it appears much less well organized [16]. Additionally, the distribution of several BMC components, namely F-actin, cadherin, and $\beta 1$ integrin, alters as fiber ends approach their sutural destinations [16,17]. These molecular rearrangements are spatially and temporally correlated with the process of fiber-end migration and appear to be necessary for accurate adhesion, de-adhesion, and translocation of fiber ends, and eventual suture formation.

The Royal College of Surgeons (RCS) rat is a model of retinal degenerative disease and subsequent posterior subcapsular cataract (PSC) formation wherein the basal fiber ends of elongating lens fibers are affected by a growth malformation [18-20]. To date, the contribution of fiber-end migration to this pathological process has not been completely elucidated. A previous study on the RCS rat has revealed distinct alterations in the F-actin arrangement and fiber-end morphology between 2 weeks and 8 weeks postnatal [21]. These changes temporally correspond to the retinal degeneration seen in this animal model. The earliest change noticed was abnormal suture sub-branch formation that subsequently led to opacity formation. The documented changes indicate that a secondary effect of the retinal dystrophy seems to be a misdirection of fiber-end migration leading to altered fiber-end morphology, F-actin rearrangements, and eventual PSC formation. The prior evidence [21] led to the hypothesis that reorganization of BMC architecture could lead to detriments in adhesion mechanics involving cell-cell attachment, cell-matrix interactions, and timely fiber-end detachment. The present study was undertaken to elucidate alterations or redistributions of select BMC components that, together with the F-actin rearrangements, might herald PSC formation.

The molecular defect that underlies the retinal dystrophy in RCS rats as well as in retinitis pigmentosa is a deletion in the gene encoding the receptor tyrosine kinase *merck* [22] and its human ortholog *MERTK* [23] [24], respectively. To date, *merck* expression has not been established in the crystalline lens. Therefore, it is likely that the migrational changes leading to cataractogenesis occur secondary to the retinal degeneration. Recent evidence has shown that *merck* is involved in an inhibitory pathway in toll-like receptor activation and that inhibition of *merck* can enhance inflammatory response [25]. In addition, microglial cell infiltration of the degenerating outer nuclear layer of RCS rat retinas is correlated with an increase in gene expression of several cytokines within the retina [26]. As stated above, the structural compromise in RCS rat lenses is primarily manifested

in the most superficial or elongating fibers at the back of the lens, resulting in PSC formation. The juxtaposition of the inflamed retina with the lens posterior suggests that PSCs could result from retinal influences via the vitreous humor. Thus, a secondary goal of the present study was to determine if cytokine levels were elevated within the vitreous humor before and during the process of PSC formation in RCS rats.

METHODS

Animals: The current study used a total of 80 RCS rats between 2 and 8 weeks of age. RCS rat breeding pairs (RCS/Lav [inbred, pink-eyed, dystrophic] and RCS-rdy⁺/Lav [genetically matched controls]) were acquired courtesy of Dr. M. LaVail, Retinal Degeneration Rat Model Resource (RDRMR), University of California, San Francisco. Animals were housed in the Comparative Research Center (CRC) of Rush University Medical Center (RUMC), Chicago, IL, and bred as per the schemata laid out by the RDRMR for breeding RCS strains. The animals were cared for in accordance with the ARVO Statement for the Use of Animals in Ophthalmic and Vision Research, and all experiments were performed under aseptic and sterile conditions as approved by the Institutional Care and Use Committee (IACUC) of RUMC. The RCS dystrophic animals were randomized into six groups (2, 3, 4, 5, 6, and 7-8 weeks), and genetically matched controls were randomized into three groups (2-3 weeks, 4-6 weeks, and 7-8 weeks), with eight animals in each group. At the predetermined age points, animals were euthanized with an intraperitoneal dose of sodium pentobarbital (1 ml at 398 mg/ml; Virbac, St. Louis, MO).

Collection of vitreous humor and lens fixation: Immediately following euthanasia, the eyes were enucleated and a small incision was made in the posterior sclera at the optic nerve origin. The vitreous was carefully collected by pipetting and was centrifuged at 11357 $\times g$ for 20 min. The supernatant was pipetted out and stored at -80 °C for eventual analyses via a multiplexed bead-based immunoassay and flow cytometry. Lenses were dissected from the orbit under a stereoscopic zoom microscope (Nikon SMZ1500; Nikon Instruments, Inc., Melville, NY), then fixed in 3% paraformaldehyde in 0.07M PBS (Sorensen's Phosphate Buffer + 0.9% NaCl).

Vibratome sectioning: Prior investigations have established that the RCS rat PSC results from a growth malformation that begins centrally (near the posterior pole) and enlarges peripherally [19]. Therefore, posterior polar vibratome sections were used in order to examine the distribution of BMC components of elongating fibers in the affected region. These sections contain intact migrating fiber ends at the capsule-fiber interface [27].

To obtain posterior polar sections, fixed lenses were secured on specimen mounting blocks, posterior side up, using cyanoacrylate adhesive, embedded in 2.5% agarose gel, and sectioned at 100 μm thickness (Figure 1A) using a vibrating knife microtome (Vibratome Series 3000 Plus-Tissue Sectioning System, Leica Biosystems, Richmond, IL). In this orientation, the first section yields the enveloping posterior capsule, the posterior fiber ends of elongating fibers, and the nascent suture branches as well as several underlying growth shells of cortical maturing fibers (Figure 1B). In subsequent sections, intact posterior fiber ends are located only beneath the beveled edge of the section where the capsule is present (Figure 1B). The basal fiber ends and thus the BMC can be visualized en face beneath the uncut posterior lens surface of section 1 (Figure 1C, blue dashed line). Intact basal fiber ends are also present beneath the beveled edge of all subsequent sections (Figure 1C, green and red dashed lines) but are typically visualized in oblique optical section due to the angle of the beveled edge. Posterior polar sections were processed for immunocytochemistry to visualize F-actin, cadherin, β -integrin, and vinculin in the BMC. 4',6-diamidino-2-phenylindole (DAPI) was also used to assay for the presence of cell nuclei in basal fiber ends in selected sections. As a positive control for the presence of nuclei, lenses from several dystrophic and genetically matched control animals were mounted anterior side up, and anterior polar vibratome sections were cut and labeled with DAPI.

Immunocytochemistry: All lens sections were fixed for an additional 30 min in 3% paraformaldehyde, permeabilized with 0.2% Triton X-100 for 30 min, and labeled for select BMC molecules. RCS rat lens sections were incubated in 10% blocking solution for 1 h to block nonspecific staining (blocking solution prepared using donkey serum (Sigma-Aldrich, St. Louis, MO) and then incubated with primary antibody cocktail overnight at 4 °C. The primary antibody cocktail used included anti-pancadherin raised in mouse at 1:100 dilution and anti-vinculin raised in rabbit at 1:50 dilution, or anti-pancadherin raised in mouse at 1:100 dilution and anti- β integrin raised in rabbit at 1:50 dilution (Sigma-Aldrich, St. Louis, MO). Sections were then thoroughly washed in blocking solution and incubated with the corresponding secondary antibody cocktail that included donkey anti-mouse immunoglobulin G (IgG) 7-amino-4-methylcoumarin-3-acetic acid (AMCA) conjugate (R & D Systems, Minneapolis, MN) and donkey anti-rabbit IgG NL493 conjugate (Jackson Immuno Research Laboratories, Inc., West Grove, PA) for 2 h.

After secondary antibody incubation, sections were washed in 0.07 M PBS and incubated in phalloidin-tetramethyl rhodamine iso-thiocyanate (TRITC) or phalloidin-fluorescein Isothiocyanate (FITC) at a 1:100 dilution of a methanolic stock (Sigma-Aldrich) for 30 min to visualize F-actin. Sections were then re-washed, and labeled sections were mounted on glass coverslips (Fisherbrand; Fisher Scientific, Pittsburgh, PA) with Vectashield mounting medium (Vector Laboratories Inc., Burlington, CA) to prevent photobleaching. Sections were always mounted with the capsule (and underlying fiber ends) facing the coverslip to provide optimal visualization of the BMC in the en face orientation. The coverslips were sealed to glass slides using a commercially available lacquer. Because some severely affected lenses displayed irregularly shaped immunofluorescent plaques that resembled nuclei, selected anterior-polar and posterior-polar sections were labeled with phalloidin-FITC+DAPI to determine if nuclei were actually present posteriorly in severely damaged lenses.

Confocal microscopy: Specimens were examined on either a Zeiss LSM 510 or Zeiss LSM 510 Meta laser scanning confocal microscope (Carl Zeiss, Jena, Germany) in the core facility of the Research Resource Center (University of Illinois at Chicago). Single-plane images, 1 μm optical thickness, were acquired at 10X, 40X, and 60X magnifications; the pinhole setting was adjusted to 1 for each magnification. Gain settings were standardized at 10%; resolution was 1024 x 1024 pixels; scan speed was 5-6; averaging=8. Contrast and brightness settings were optimized individually for each image. Laser scanning confocal micrographic (LSCM) images were viewed and analyzed using the Zeiss LSM Image Browser version 2.30.011 (Carl Zeiss) and Adobe Photoshop version 7.0 (Adobe Systems Inc., San Jose, CA). Our prior analysis of BMC architecture in normal rat lenses [16] determined that basal fiber ends are "boutons" having a depth of approximately 4 μm from the capsule-fiber interface (CFI) to the lateral borders of underlying fibers. Therefore, all localization of BMC components was performed within these parameters by first performing a through-focus z-series beginning at the CFI. Only focal planes that were within the stated parameters of the BMC (<4 μm deep to the CFI) were imaged. As stated above, PSCs in the RCS rat begin forming centrally (at the posterior pole) and enlarge peripherally. Therefore, fiber ends in the sutural, perisutural, and distal area of the lateral-posterior region of fiber-end migration [17] were examined in this study since these comprise the areas affected by growth malformation. These areas are delineated with blue, green, and red dotted lines in Figure 1C.

Intravitreal cytokine analysis using multiplexed bead-based immunoassay and flow cytometry: The vitreous samples that

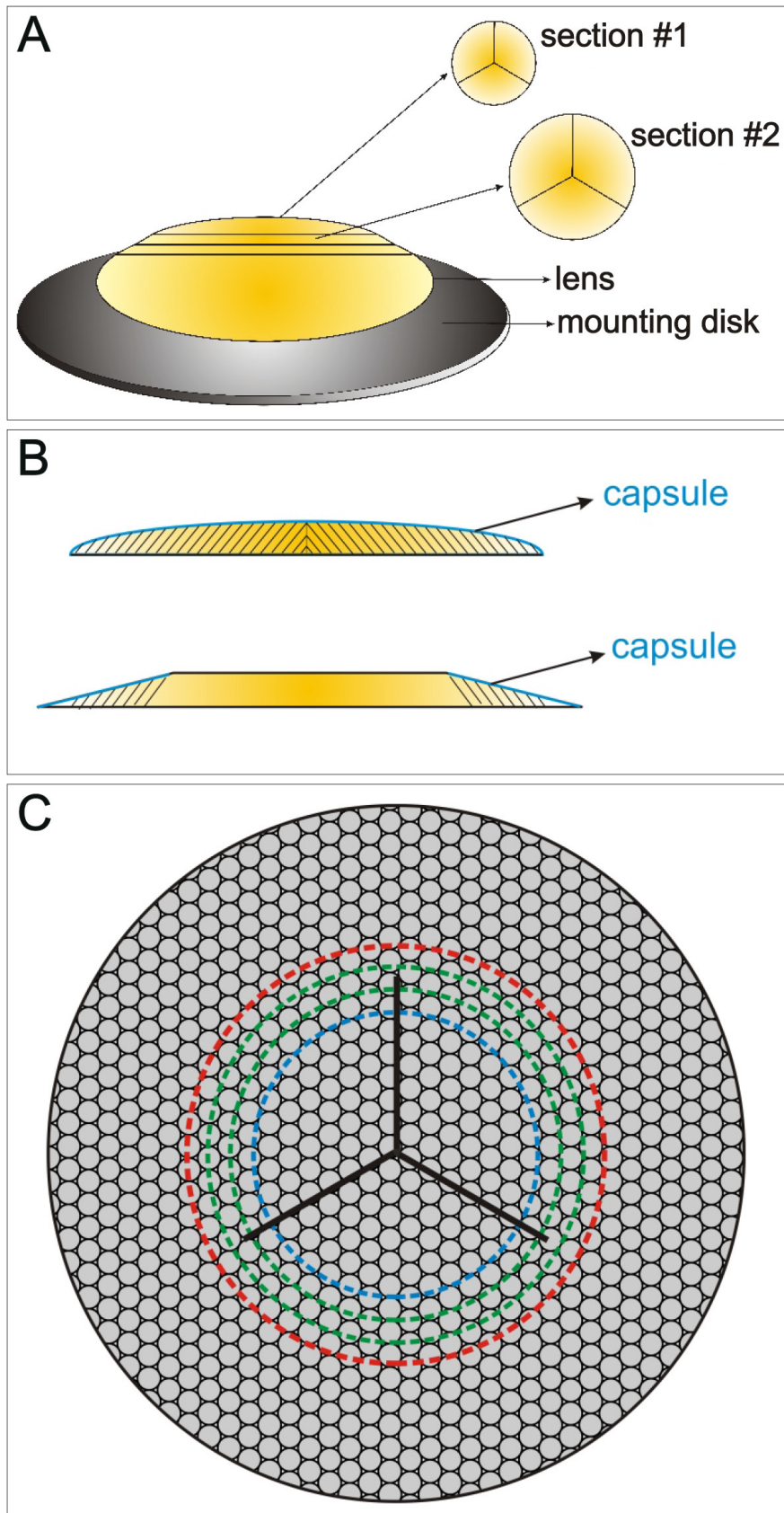


Figure 1. Diagrammatic representation of the orientation of vibratome sections, location of intact posterior fiber ends, and region where imaging of the BMC was performed. **A:** Posterior polar sections were obtained with a vibrating knife microtome, yielding serial sections of increasing diameter. **B:** An enlarged edge-on view of the first two sections demonstrates the location of intact migrating basal fiber ends. In the initial section, intact basal fiber ends were present beneath the entire curved surface of the enveloping capsule, whereas all subsequent sections only had intact fiber ends beneath the beveled edge covered by the capsule. Sections are not to scale. **C:** Enlarged en face view of the posterior surface of the lens shows basal fiber ends beneath the capsule in the first section (blue dashed line) and in subsequent sections (green and red dashed lines). The regions of fiber-end migration where the BMC architecture was imaged are encompassed within the outermost red dashed line and comprise the distal portion of the lateral-posterior region, the perisutural region, and the sutural region.

were collected from RCS rat lenses were processed as per the manufacturer's instructions and analyzed for the presence of inflammatory cytokines (specifically, interleukin [IL]-1 α , IL-4, IL-6, IL-8, tumor necrosis factor [TNF], and interferon [IFN]- γ) using the BD-Cytometric Bead Array (BD-CBA; Becton Dickinson, San Jose, CA). The BD-CBA is a multiplexed bead-based immunoassay that uses a series of spectrally discrete particles to capture and quantitate soluble analytes. Specifically, the antibody-coated beads were reacted with the analyte (soluble antigen), and the solution was then incubated with the detector antibody, which was directly labeled with phycoerythrin. After washing to remove any excess antibodies or beads, the levels of the analyte were measured by detecting the antibody-antigen-bead complex using a flow cytometry application to detect the fluorescence-based emission. The data were acquired on an LSR II flow cytometer (Becton Dickinson) followed by analysis using the BD-FCAP software (BD Biosciences, San Jose, CA). The data were subjected to analysis (Student *t* test) to determine whether there was a statistically significant difference between control and age-matched dystrophic animals for each of the six cytokines analyzed. A *p* value of $p \leq 0.05$ was considered significant.

RESULTS

Control (RCS-rdy⁺/Lav) lenses: The distribution of select BMC components in RCS control animals did not alter as a function of age, rather consistent labeling patterns were seen at all ages examined. Vinculin was present as discrete spots on the cell membrane at the junctions between the fiber ends (Figure 2A, arrowheads), in keeping with its presence in focal adhesion complexes. Vinculin was seen closely associated with F-actin, which outlined the fiber ends, indicating its role in anchoring F-actin to the membrane (Figure 2A, arrows). As expected, β integrin in the control animals was visualized as a plaque within the fiber ends (Figure 2B, asterisks). The periphery of the BMC was outlined with F-actin, and integrin was co-localized with F-actin at the junction of the basal and lateral membrane domains. The pattern of integrin expression exhibited in the RCS model concurs with that previously documented in normal Sprague-Dawley rat BMC [17]. Cadherin, the calcium-dependent adhesion molecule, was clearly seen outlining the fiber ends (Figure 2C). This normal distribution of cadherin, i.e., within adherens junctions, has been described in lens epithelial cells, lens fiber cells, and in the BMC by several investigators [1,7,17,28,29]. In the RCS controls, cadherin was co-localized with F-actin at the periphery of fiber ends (Figure 2D, arrows).

The distribution of the above BMC components is summarized diagrammatically in RCS control animals (Figure 3). In control (RCS-rdy⁺/Lav) animals, the peripheral distribution of F-actin (Figure 3A) and cadherin (Figure 3B) within the BMC is depicted. The punctate distribution of vinculin (Figure 3C) is shown as well as the plaque-like distribution of β integrin (Figure 3D).

Dystrophic (RCS/Lav) lenses: In contrast to the distribution seen in the RCS control animals, there were distinct alterations in the distribution of BMC components in the RCS dystrophic animals as a function of age. The changes seen can be defined temporally with the most distinct alterations being visualized at 4–6 weeks postnatal. This temporal change is consistent with the gross structural changes that occur in the RCS rat lens within the same time window [21].

2–3 weeks old: As expected from our prior studies, F-actin was distributed continuously around the BMC periphery (Figure 4A, arrows). Labeling for vinculin in RCS/Lav rat lenses at 2 weeks was comparable to the controls, with distinct foci visible—many of which appeared to be associated with membrane-linked F-actin (Figure 4A, arrowheads). Cadherin also was found to delineate the ends clearly (Figure 4B, arrows) comparable to its arrangement in the BMC of controls. β integrin had a completely different distribution as compared to the controls as early as 2 weeks postnatal. Instead of being present as a plaque within the BMC, β integrin was arranged as discrete spots (Figure 4C, arrowheads). These spots continued to be present on the membranes, but the co-localization with F-actin that was seen in the normal controls was absent.

4–6 weeks old: As previously described [21], the F-actin distribution in the BMC of 4-week-old dystrophic rat lenses was significantly altered so that foci of F-actin (Figure 5A, arrowheads) were present within the continuous peripheral distribution. By 5–6 weeks postnatal, the F-actin foci were more prominent (Figure 5D, arrowhead) and were arranged in a “rosette” pattern (Figure 5F, arrows). Cadherin, continued to outline the BMC in lenses from 4-week-old dystrophic rats, and discrete foci of cadherin were also seen along the perimeter of the fiber ends (Figure 5B, arrowheads) where they were co-localized with F-actin (Figure 5C). Although cadherin continued to be co-localized with F-actin in 6-week-old lenses, it also appeared to be present in the cytoplasm of fibers within the developing PSC (Figure 5H-I, stars). By 4 weeks postnatal, vinculin was present as a diffuse stratum within the BMC and was outlined by F-actin rosettes (Figure 5E, asterisks); this distribution was noted through 6 weeks of age. At 4 weeks postnatal, β integrin was configured similar to the pattern seen at 2–3 weeks (similar to Figure 2C; data

not shown); however, its distribution altered by 6 weeks of age. Specifically, although labeling for β integrin showed faint cytoplasmic fluorescence, it was also clearly distinguishable around BMC profiles and at lateral membranes as a continuous fluorescence where it was co-localized with F-actin (Figure 5G, arrows).

7–8 weeks old: At 7–8 weeks of age, fiber-end morphology within the PSC plaque was consistent with our prior observations [21] and the distribution of BMC components was consistent for the majority (approximately 75%) of RCS dystrophic animals. Specifically, F-actin was distributed around the aberrantly enlarged and irregular posterior fiber ends (Figure 6A). F-actin foci persisted in most lenses; however, some profiles displayed diffuse cytoplasmic labeling in addition to the foci (Figure 6D, stars). Fully formed PSC plaques precluded the formation of posterior sutures; this damage was propagated inward, affecting fibers and suture planes several layers deep to the capsule (Figure 6B). Labeling for cadherin continued to display faint cytoplasmic fluorescence (Figure 6C, asterisks), with more definitive labeling at the

BMC periphery. Small punctate foci of immunofluorescence for vinculin was present around the border of excessively dilated fiber ends (Figure 6E, arrowheads) within the PSCs. Integrin distribution in fiber ends of dystrophic animals was comparable to that seen in 6-week-old dystrophic lenses (data not shown).

The temporal sequence of alterations in the distribution of the above BMC components is summarized diagrammatically in (Figure 7 and Figure 8). F-actin (Figure 7A-D) is depicted in red and was initially distributed around the periphery of the BMC (Figure 7A) but by 4 weeks postnatal was altered such that foci were visible at vertices (Figure 7B). The F-actin foci became more prominent as the PSC developed and persisted through 8 weeks postnatal in the majority of lenses (Figure 7C-D). Cadherin (Figure 7E-H) is depicted in blue and was almost completely co-localized with F-actin in 2- and 4-week-old dystrophic lenses (Figure 7E-F); however, its distribution became increasingly diffuse and cytoplasmic during PSC progression (Figure 7G-H). Vinculin (Figure 8A-D) is depicted in gold. At 2 weeks

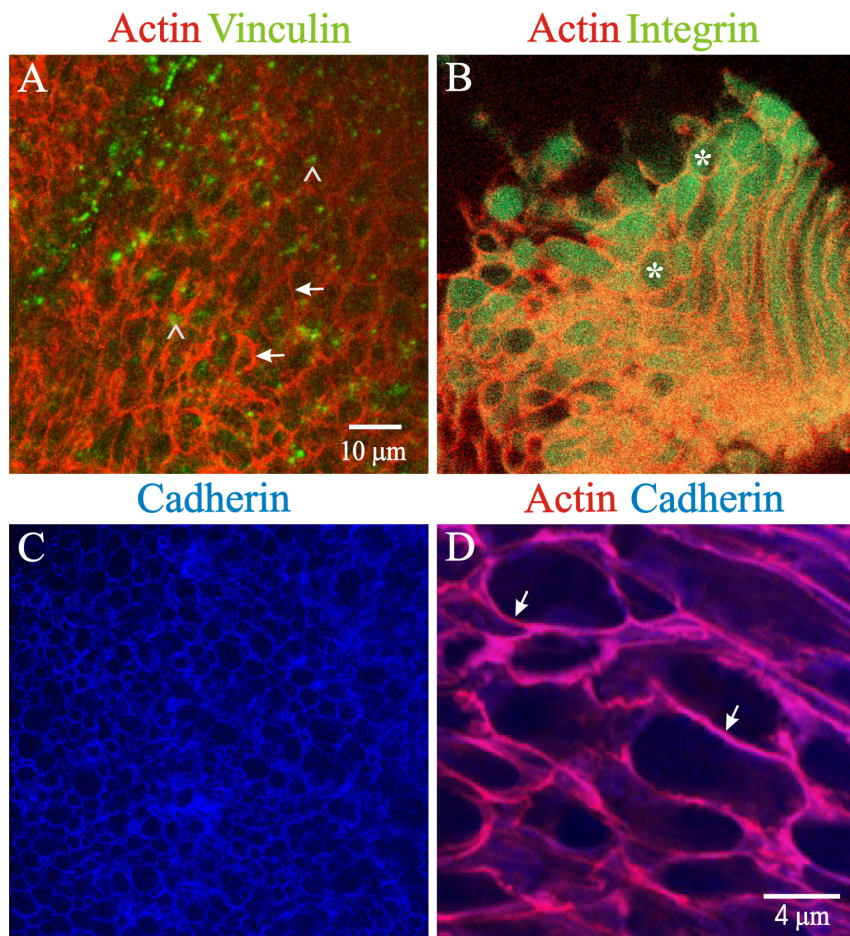


Figure 2. LSCM images of 2–6-week-old RCS-rdy⁺/Lav (control) posterior fiber ends in the en face orientation. In control rat lenses the distribution of F-actin, vinculin, cadherin and integrin did not alter as a function of age. **A:** A 2-week-old animal. Vinculin was present as discrete spots located at cell membranes (arrowheads) and was closely associated with F-actin, which outlined the fiber ends (arrows). **B:** A 4-week-old animal. β integrin in the control animals was distributed as a plaque within fiber ends (asterisks). **C:** A 3-week-old animal. Immunofluorescence for cadherin was present at the BMC periphery. Panels A–C are at the same magnification. **D:** A 6-week-old animal. Double labeling for F-actin and cadherin demonstrated that both components were localized at the periphery of the BMC and demonstrated a high degree of co-localization (arrows).

postnatal, vinculin was distributed as scattered punctate spots (Figure 8A); however, this pattern was altered by 4 weeks postnatal. Specifically, many fiber ends displayed diffuse vinculin immunofluorescence within the BMC, and this pattern persisted through 6 weeks postnatal (Figure 8B-C). In 8-week-old dystrophic lenses, immunofluorescence for vinculin was arranged as small punctate foci around the border of distended basal fiber ends within the PSC plaque (Figure 8D). The distribution of β integrin (Figure 8E-H) is depicted in green. At 2 to 4 weeks postnatal, β integrin was distributed as discrete spots, often coincident with the BMC borders (Figure 8E-F). However, in lenses from 6- to 8-week-old dystrophic rats, faint immunofluorescence for β integrin was present in the cytoplasm and to a greater degree around the periphery of basal fiber ends (Figure 8G-H).

A sub-set (~25%) of the 7–8 week dystrophic lenses was severely damaged (Figure 9). In those lenses, basal fiber-end morphology was altered to form “stellate”-shaped ends as formerly shown [21]. F-actin was strongly localized to the

stellate “arms” of the fiber ends (Figure 9A,D,F, arrows). Labeling for integrin (Figure 9C-D) had a diffuse distribution with more pronounced labeling in the stellate arms where it was co-localized with F-actin. Cadherin distribution was drastically altered; it no longer outlined the fiber ends, instead cadherin was now present as irregularly shaped plaques between stellate projections within the fiber ends (Figure 9B, asterisks). As such, it was no longer co-localized with F-actin. Because the altered cadherin distribution in severely affected lenses superficially resembled nuclei, selected anterior polar and posterior polar sections were labeled with phalloidin-FITC+DAPI to determine if nuclei were indeed present. Anterior polar sections displayed DAPI-positive ovoid nuclei (Figure 9E, stars) surrounded by cytoplasmic F-actin, consistent with the presence of anterior epithelial cells. In contrast, no DAPI-positive structures were detected in posterior polar sections of severely affected dystrophic lenses (Figure 9F). Additionally, the cadherin-positive plaques were more irregular in size and shape than the nuclei of lens epithelial

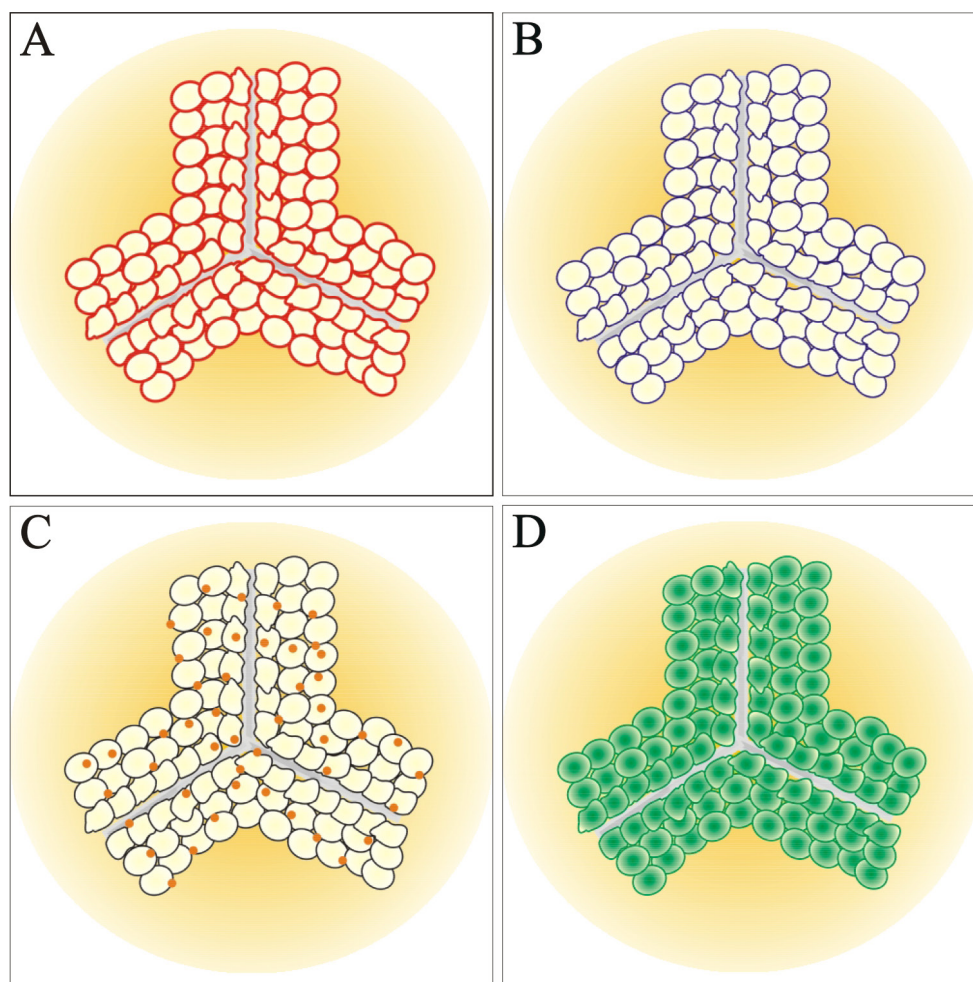


Figure 3. Diagram summarizing the distribution of various BMC components in migrating fiber ends of RCS-rdy⁺/Lav (control) rats. **A:** F-actin is shown in red; **B:** cadherin is shown in blue; **C:** vinculin is shown in gold; **D:** β integrin is shown in green. Both F-actin and cadherin were localized to the periphery of the BMC. Vinculin was distributed as scattered punctate spots, whereas β integrin had a diffuse plaque-like distribution within the BMC.

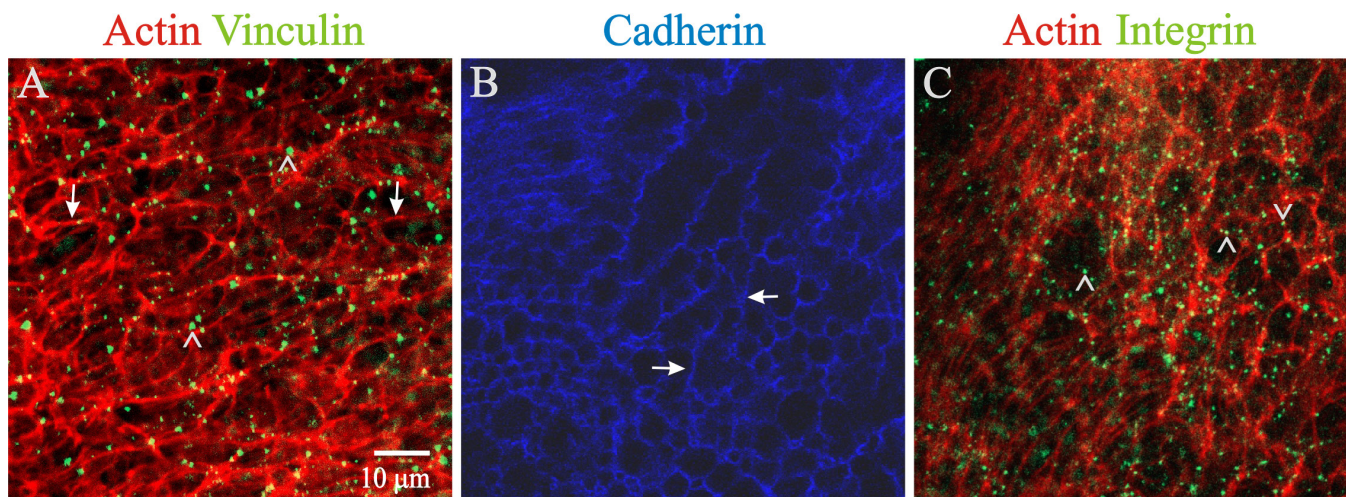


Figure 4. LSCM images of 2–3-week-old RCS/Lav (dystrophic) posterior fiber ends viewed en face. **A, B, C:** In dystrophic rat lenses from 2 to 3 weeks old, distribution of F-actin (**A** and **C**), vinculin (**A**), and cadherin (**B**) was comparable to controls; however, integrin distribution (**C**) was altered. Specifically, F-actin and cadherin outlined the BMC (**A** and **B**, arrows), whereas, vinculin was present in discrete spots (**A**, arrowheads). Controls displayed a plaque-like integrin distribution in the BMC, whereas dystrophics had a random punctuate pattern (**C**, arrowheads). Panels **A–C** are at the same magnification.

cells, further differentiating them from nuclei (compare Figure 9B,E).

Intravitreal inflammatory cytokines: A multiplexed bead based analysis was used to measure the levels of select inflammatory cytokines within the vitreous in RCS-*rdy*^{+/} Lav and RCS/Lav rats between 2 and 8 weeks postnatal. The cytokine levels measured included IL-1 α , IL-4, IL-6, IL-8, TNF, and IFN- γ (in pg/ml); results are shown graphically in Figure 10.

In dystrophic animals, IL-1 α , IL-4, TNF, and IFN- γ demonstrated a similar pattern, with concentrations increasing between 2 and 6 weeks of age and then gradually decreasing up to 8 weeks of age. The highest intravitreal levels in dystrophic animals were attained by IL-4 and TNF in the 4–6-week age group, with average concentrations of 148.00 pg/ml and 34.20 pg/ml, respectively. IL-1 α , IL-6, IL-8, and IFN- γ levels did not exceed 15 pg/ml at any time point in the vitreous humor of dystrophic animals.

In the control animals, IL-1 α concentration was below detection levels (0 pg/ml) up to 3 weeks postnatal, after which a mean level of 1.76 pg/ml was maintained up to 8 weeks postnatal. In the dystrophic animals, IL-1 α increased from a mean of 3.46 pg/ml at 2–3 weeks of age, through 4.94 pg/ml at 4–6 weeks of age, to 4.22 pg/ml at 7–8 weeks of age. The levels of IL-1 α in dystrophic animals were significantly different ($p \leq 0.05$) when compared to the control animals of the same age at all time points examined (Figure 10A).

Concentrations of IL-4 in the control animals were 12.69 pg/ml at 2–3 weeks postnatal, 47.92 pg/ml at 4–6 weeks postnatal, and 49.11 pg/ml at 7–8 weeks postnatal. In comparison, the dystrophic animals exhibited an extremely high average IL-4 concentration of 109.30 pg/ml as early as 2 weeks postnatal. IL-4 levels in dystrophic animals gradually peaked at 148.00 pg/ml by 6 weeks postnatal, then tapered to a mean of 37.61 pg/ml by 8 weeks postnatal. The levels at 2–3 weeks and 4–6 weeks in the dystrophic animals were both significantly different ($p \leq 0.05$) as compared to age-matched control animals (Figure 10B).

Intravitreal levels of IL-6 demonstrated an interesting presentation, with the dystrophic animals maintaining near constant mean levels of 4.93 pg/ml from 2 weeks through 8 weeks postnatal. Control animals had a mean IL-6 concentration of 0.80 pg/ml at 2 weeks of age, which rapidly decreased to nearly undetectable levels at 4 weeks and was 0.04 pg/ml by 8 weeks of age (Figure 10C). The IL-6 levels in the dystrophic animals were significantly different ($p \leq 0.05$) as compared to control animals at all ages examined.

Concentrations of IL-8 in the vitreous showed a completely different pattern of presentation when compared to the other tested cytokines. IL-8 levels in the dystrophic animals were maintained at a mean of 1.83 pg/ml up to 6 weeks of age and then showed an abrupt increase to 6.91 pg/ml at 7–8 weeks of age. The control animals had a uniformly low concentration of IL-8 (<1 pg/ml) at all ages examined. There was no significant difference between dystrophic and

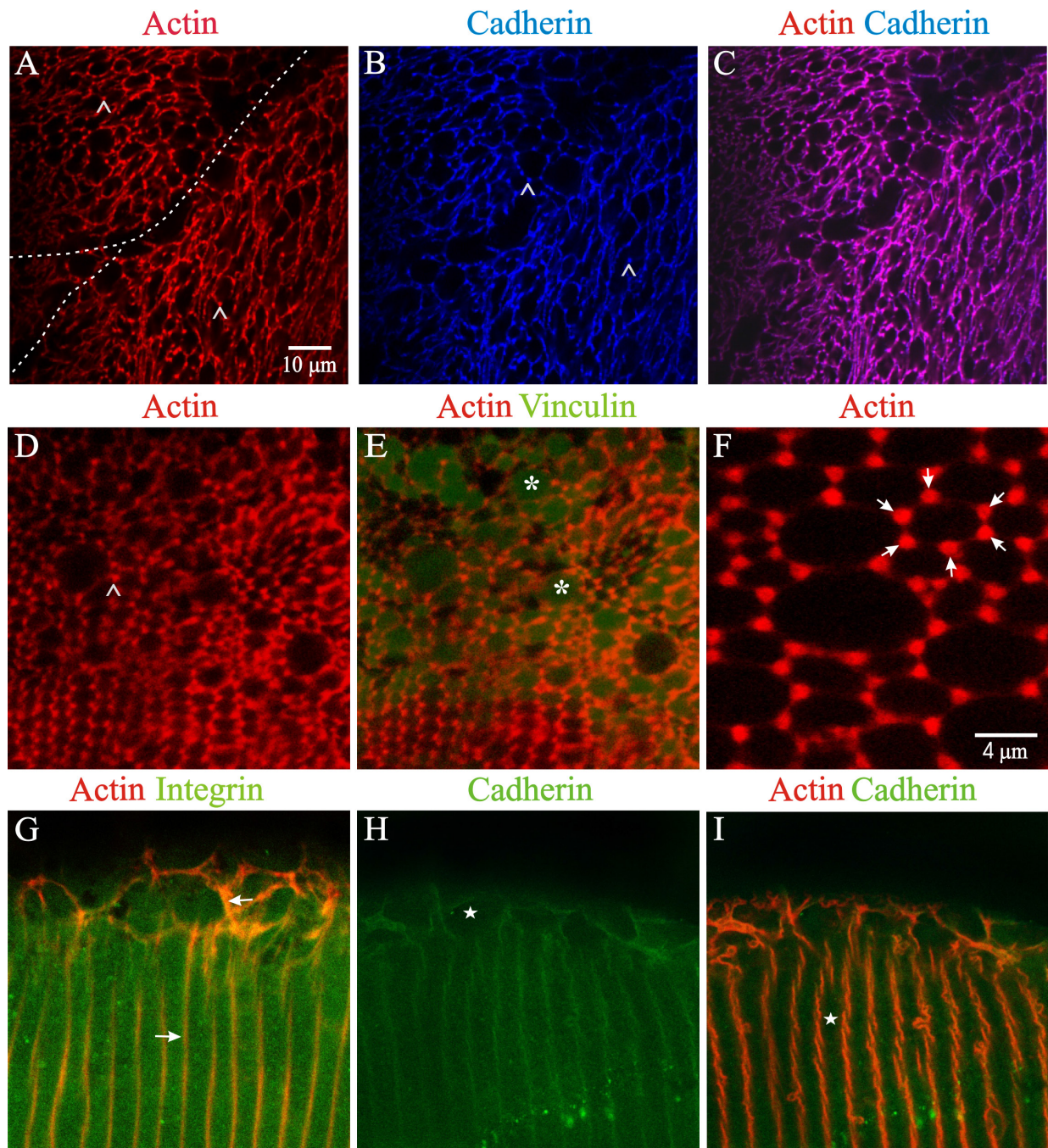


Figure 5. LSCM images of RCS dystrophic rat lenses at 4–6 weeks postnatal. **A, B, C:** The same field of view showing an en face view of fiber ends in 4-week-old animals labeled for F-actin (**A**, arrowheads), cadherin (**B**, arrowheads), and the merged image (**C**). F-actin and cadherin were almost completely co-localized (**C**) around the perimeter of the BMC. The formation of the previously described F-actin foci [21] was discernible. A portion of a suture branch with abnormal sub-branching is delineated by a dashed white line. **D, E:** The same field of view showing F-actin (**D**) and the merged F-actin/vinculin double label (**E**) in the en face orientation. Within the forming PSC of 5-week postnatal animals, distinct F-actin foci (arrowheads) were present around the BMC perimeter with vinculin rearranged as diffuse plaques (asterisks). **F:** An en face view at high magnification clearly showed the rosette arrangement of F-actin (arrows) by 6 weeks postnatal. **G:** An oblique optical section of a 6-week-old lens shows that β integrin had a diffuse distribution as well as a more pronounced presence in the lateral membranes and BMC periphery (arrows), which was partially co-localized with F-actin. **H, I:** The same field of view showing cadherin (**H**) and the merged cadherin/actin (**I**) double label in an oblique optical section from a 6-week-old lens. Similar to β integrin, cadherin showed a more dispersed labeling pattern (stars) than at earlier time points. Panels **A–E** and **G–I** are at the same magnification.

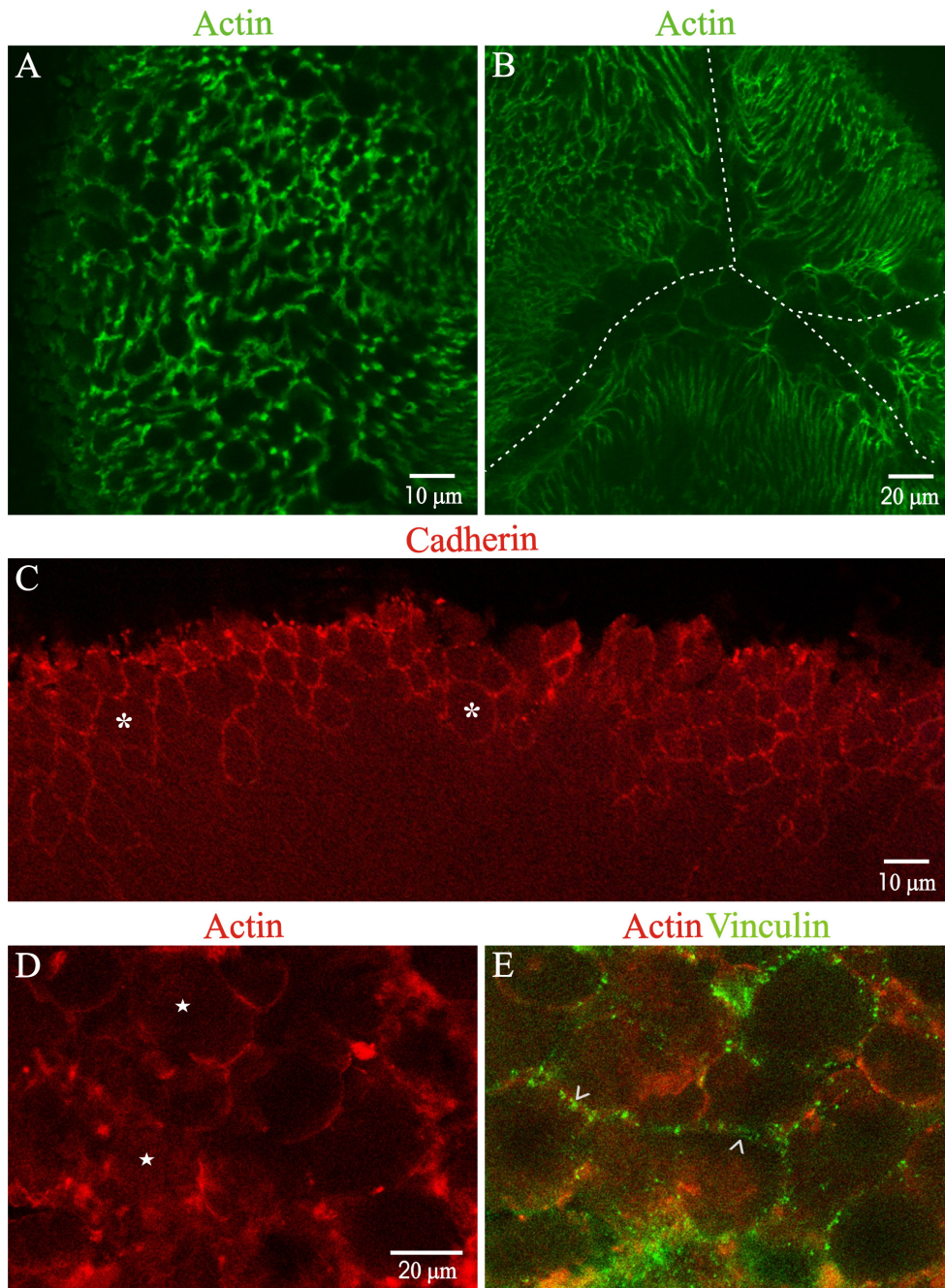


Figure 6. LSCM images of typical RCS dystrophic lenses at 7–8 weeks postnatal. All images are viewed en face. **A:** In most lenses (~75%) the F-actin foci were noted within the PSC plaque. **B:** An optical section approximately 10 μm deep to the capsule–fiber interface. Fiber ends adjacent to and at posterior sutures (dashed white lines) were excessively dilated, resulting in disruption of sutures deep to the migrating fiber ends. **C:** Cadherin distribution was comparable to 6-week-old lenses, i.e., it displayed a diffuse distribution (asterisks) in the BMC with more pronounced punctate labeling at the periphery. **D, E:** The same field of view showing F-actin (**D**) and the merged F-actin/vinculin image (**E**). Extremely dilated fiber ends within the plaque frequently had a mottled labeling pattern for F-actin (stars) and weak punctate fluorescence for vinculin around the periphery (arrowheads). Panels **D** and **E** are at the same magnification.

age-matched control animals for this cytokine between 2 and 8 weeks of age (Figure 10D).

Concentrations of TNF as a function of age in the dystrophic animals followed a pattern similar to that seen with IL-1 α and IL-4 levels. Specifically, at 2 weeks of age, dystrophic animals had a mean concentration of 27.02 pg/ml, which rose to 34.20 pg/ml at 4–6 weeks of age. By 7–8 weeks postnatal, the TNF intravitreal concentration in dystrophic animals began to decline and had a mean concentration of

26.20 pg/ml. The control animals demonstrated a mean level of 7.71 pg/ml between 2 and 8 weeks postnatal. Statistical analysis revealed that the mean levels of TNF in dystrophic animals were significantly different ($p \leq 0.05$) when compared to age-matched controls from 2 to 8 weeks of age (Figure 10E).

Intravitreal levels of IFN- γ were below detectable levels (0 pg/ml) in the controls at 2–3 weeks of age. These levels slowly increased to 0.20 pg/ml at 4–6 weeks and 2.15 pg/

ml by 7–8 weeks of age. The average IFN- γ levels in the dystrophic animals were 2.99 pg/ml at 2–3 weeks, 5.38 pg/ml at 4–6 weeks, and 3.53 pg/ml at 7–8 weeks. At all ages tested (2–8 weeks postnatal), the mean concentration of IFN- γ was significantly higher ($p \leq 0.05$) in dystrophic as compared to age matched control animals (Figure 10F).

DISCUSSION

The present study evaluates temporal changes in distributions of vinculin, cadherin, and β integrin in the BMC of RCS rats during abnormal fiber-end migration leading to PSC formation [21]. In the lens, vinculin is typically enriched along the lateral membranes and in the BMC as they approach the sutures [30]. Adhesion complexes in the normal lens undergo remodeling during fiber-cell maturation to stabilize fiber-cell contacts [30]. In the RCS rat (by 4 weeks postnatal), the remodeling results in vinculin staining becoming more prominent along the lateral membranes as they approach the sutures, indicating a strong interaction between adjacent fiber cells during fiber-end migration. The rearrangement of vinculin in the RCS dystrophics seems to indicate a reversal of the stabilization seen in normal lenses. Instead of vinculin “securely holding” the fiber ends together within

the basolateral membranes, the diffuse distribution might be contributing to decreased adhesion dynamics between the fiber cells, eventually leading to abnormal suture sub-branch formation and PSCs in these animals [21]. Since vinculin is responsible for linking integrin to the F-actin cytoskeleton, its rearrangement could result in the concomitant alteration in integrin distribution that was seen as early as 2 weeks postnatal in the RCS rats.

Focal adhesion complexes not only ensure adhesion but are also responsible for accurate positioning of actin filaments and targeting of signaling molecules. Integrin-actin interaction is essential for establishing cell polarity, directed-cell migration, and maintenance of cell growth and survival [31], and a loss of this interaction can result in de-adhesion and can affect directed cell migration in other cell types, specifically in wound healing [32]. In the lens, de-adhesion of the fiber cells, specifically at the basolateral domains, would mean a lack of interaction between adjacent fiber ends within a growth shell as well as between growth shells, potentially resulting in a lack of cell–cell communication that is responsible for directed fiber-end migration and leading to a breakdown of structural integrity and eventual PSC formation. In the RCS model, although integrin continued to

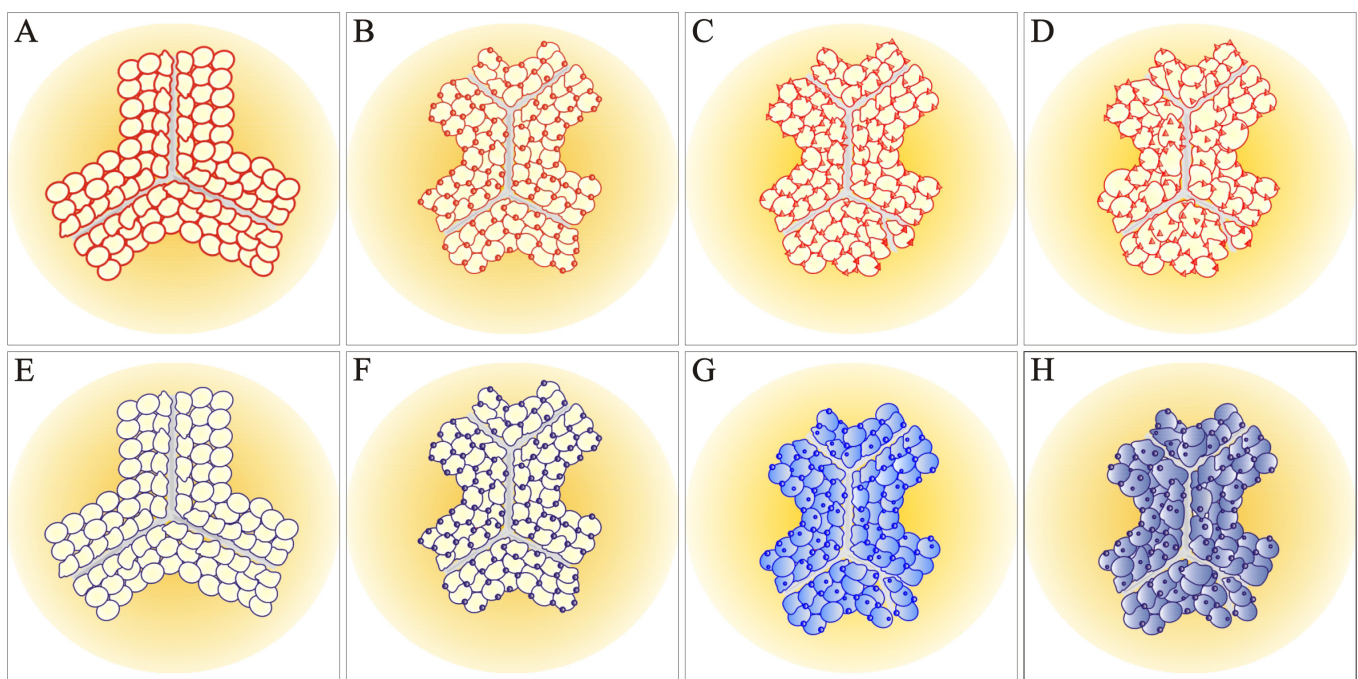


Figure 7. Diagram summarizing the distribution of F-actin (shown in red; **A–D**) and cadherin (shown in blue; **E–H**) in the BMC of migrating fiber ends in RCS/Lav (dystrophic) rats. **A, E:** At 2 weeks old; **B, F:** at 4 weeks old; **C, G:** at 6 weeks old; **D, H:** at 8 weeks old. F-actin was initially distributed around the periphery of the BMC but by 4 weeks postnatal was altered such that foci were visible at vertices. The F-actin foci became more prominent as the PSC developed and persisted through 8 weeks postnatal in the majority of lenses. Cadherin was almost completely co-localized with F-actin in 2- and 4-week-old dystrophic lenses; however, its distribution became increasingly diffuse and cytoplasmic during PSC progression.

co-localize with F-actin in the basolateral/lateral membrane domains, the lack of integrin in the basal domain could be critical in maintaining the extracellular matrix (ECM) to fiber-cell communication at this interface. This could also be responsible for the transient cessation in lens growth that has been seen in this animal model [21].

The cell-cell adherens junction in cell membranes is the specialized adhesion complex formed by cadherins and densely associated with actin [33]. Cadherin distribution in avian and rodent lenses [17,34] is restricted to the lateral membrane domains and the basolateral domains. In the BMC of rodents, cadherin has been shown clearly outlining the fiber ends (only at the BMC periphery), and this was evident in the RCS dystrophics up to 5 weeks postnatal, after which cadherin was also seen in the cytoplasm and at the basal membrane domain. In addition to the mechanical properties associated with adherens junctions as a virtue of their intimate association with actin bundles, cadherins also play a critical role in cell growth and transmembrane signaling, specifically during differentiation, proliferation, and migration [35]. In the lens, normal cadherin arrangement facilitates

normal fiber-cell differentiation and fiber-end migration. The dynamic adhesive properties that can be attributed to the adherens junctions play a critical role in maintaining the integrity of the fiber cells as they elongate and migrate en-mass toward the sutures. In the RCS dystrophic animals, a loss of this normal cadherin configuration that occurs could be responsible for the initiation of the aberrant fiber-end migration. The redistribution of cadherin from the basolateral/lateral membrane domains into the cytoplasmic/basal domain by 6 weeks postnatal could result in altered adhesion dynamics. An increased adhesive interaction between the fiber ends at the BMC could result in a transient cessation of fiber-end migration, which could be further reflected in the slower lenticular growth rate shown in these animals.

Basement membrane and cytoskeletal molecules function as anchoring and scaffolding components in cells [36-38]. The interactions between adjacent cells as well as interactions between several BMC and cytoskeletal components acting together play an important role in maintaining normal architecture of lens fiber cells. Normal cytoarchitecture is maintained not only within each fiber but also within any cohort

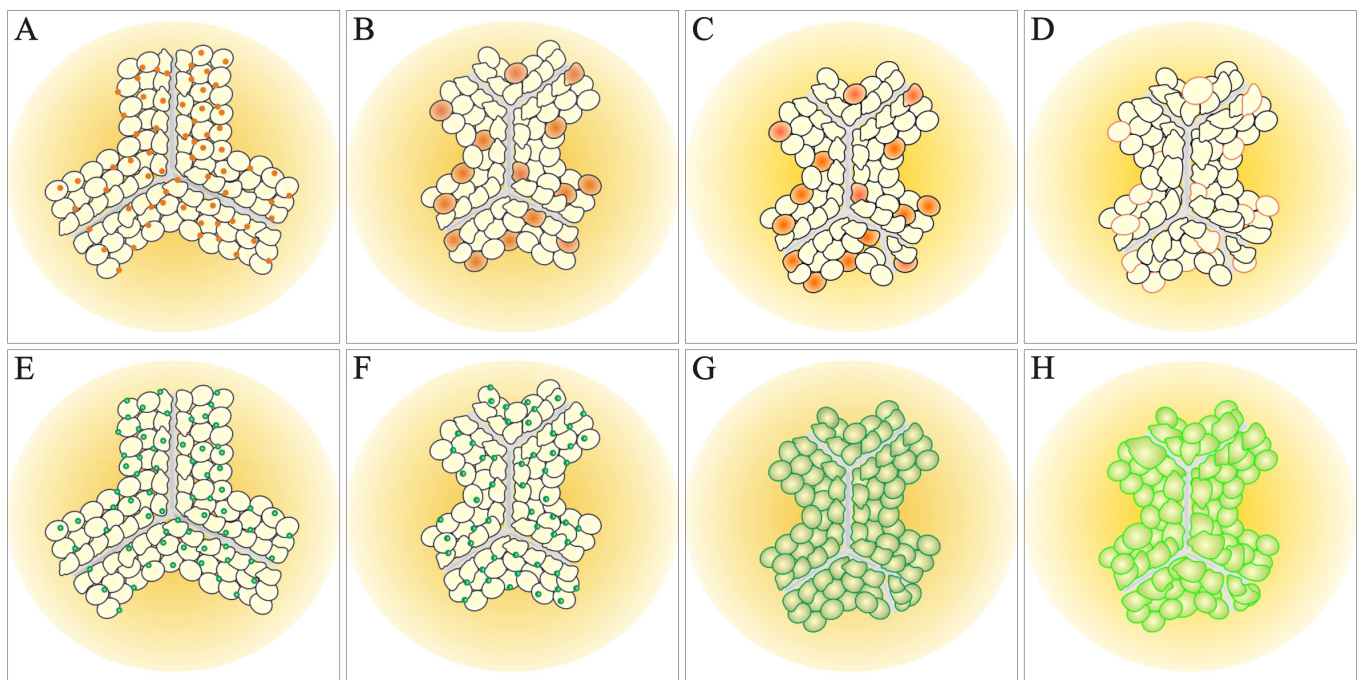


Figure 8. Diagram summarizing the distribution of vinculin (shown in gold; **A-D**) and β integrin (shown in green; **E-H**) in the BMC of migrating fiber ends in RCS/Lav (dystrophic) rats. **A, E**: At 2 weeks old; **B, F**: at 4 weeks old; **C, G**: at 6 weeks old; **D, H**: at 8 weeks old. At 2 weeks postnatal, vinculin was distributed as scattered punctate spots; however, this pattern was altered by 4 weeks postnatal. Specifically, many fiber ends displayed diffuse strata of vinculin within the BMC, and this pattern persisted through 6 weeks postnatal. In the majority of 8-week-old dystrophic lenses, immunofluorescence for vinculin was arranged as small punctate foci around the border of basal fiber ends. At 2-4 weeks postnatal, β integrin was distributed as discrete spots, often coincident with the BMC borders. However, in lenses from 6- to 8-week-old dystrophic rats, faint immunofluorescence for β integrin was present in the cytoplasm and to a greater degree around the periphery of basal fiber ends.

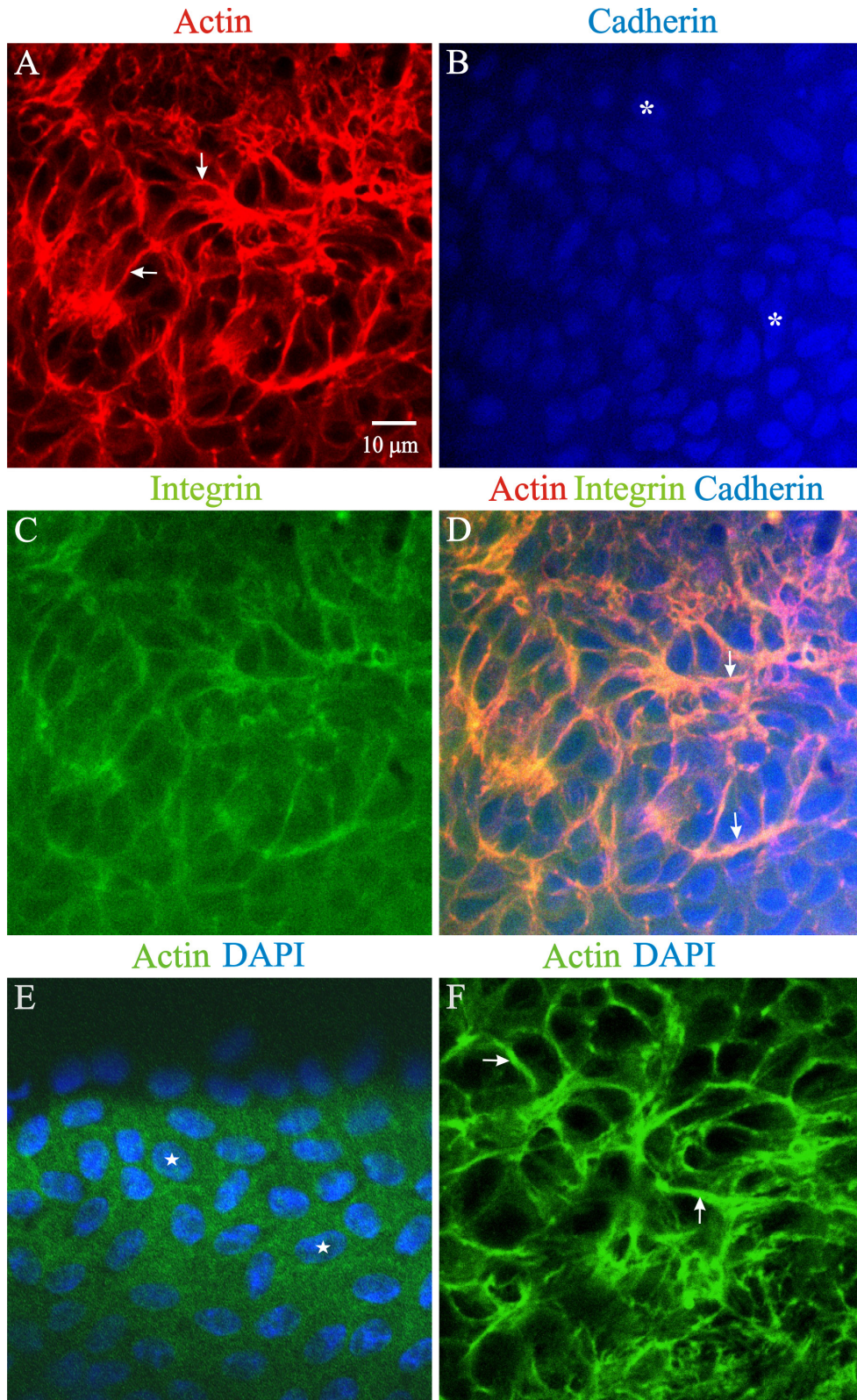


Figure 9. Representative LSCM images of severely damaged RCS dystrophic lenses at 7–8 weeks postnatal. In a subset of lenses (~25%), many posterior fiber ends adopted a stellate shape. **A–D**: The same field of view showing F-actin (**A**), cadherin (**B**), integrin (**C**), and the merged image of the triple-labeled fiber ends (**D**). Orientation is en face. F actin was localized to the stellate arms of the fiber ends (**A**, **D**, arrows); however, integrin had a diffuse distribution with more pronounced labeling in the stellate arms (**C**). Cadherin was localized to irregularly shaped plaques between stellate projections (**B**, asterisks). **E–F**: Anterior (**E**) and posterior (**F**) polar sections doubled labeled with phalloidin-FITC and DAPI demonstrate the distribution of F-actin and nuclei. Nuclei were present only in anterior sections (**E**, stars); no DAPI-positive fluorescence was present in posterior sections. F-actin was localized to stellate projections (**F**, arrows). This confirms that the cadherin-positive plaques do not represent nuclei. Panels **A–F** are at the same magnification.

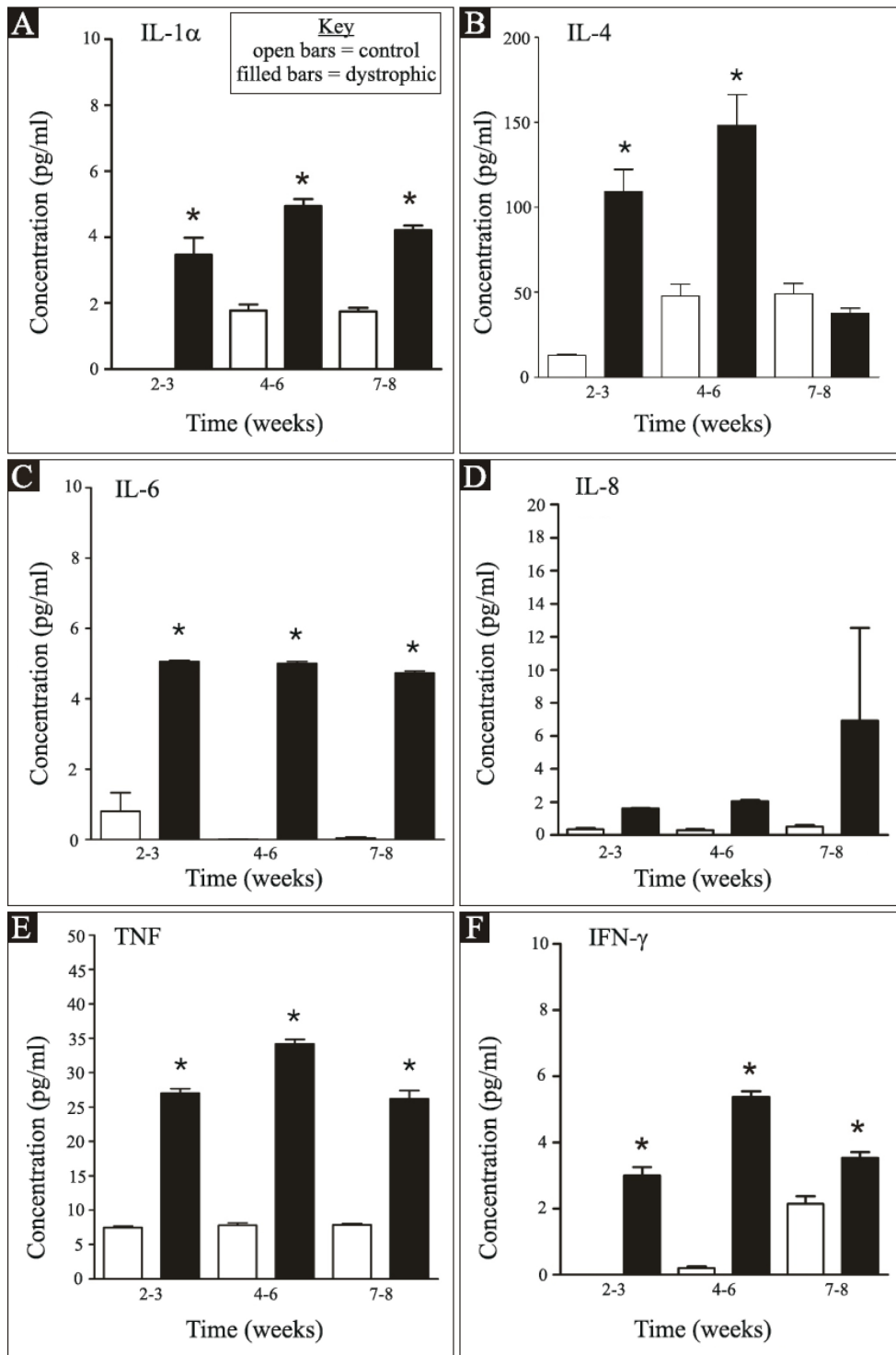


Figure 10. Bar graphs showing the intravitreal concentration of pro-inflammatory cytokines in RCS control (n=24) and RCS dystrophic (n=48) rat eyes over time. The data are plotted as mean ± standard error of the mean; * indicates significant difference between control and dystrophic groups ($p \leq 0.05$). A: IL-1 α , B: IL-4, C: IL-6, D: IL-8, E: TNF, F: IFN- γ .

of fibers taken together. This results in transparency within each lens fiber as well as within segments or layers of lens tissue, and ultimately the entire lens. In the RCS rat lenses, the alterations in F-actin are associated with altered vinculin, integrin, and cadherin arrangements. It is highly probable that the loss or disruption of normal cytoarchitecture results in the loss of lenticular transparency seen in these animals.

In addition to alterations in BMC architecture, changes in shape have also been documented in RCS lens fiber ends [21]. Cell shape alterations may be responsible for changes in cellular metabolism, cell growth, and the production of specific proteins [39-43]. The altered BMC architecture coupled with abnormal fiber-end shape could be responsible for the slower lens growth demonstrated [21]. Cellular metabolism could be affected as well and might be responsible for altered cell membrane properties. The production of lens-specific crystallins could be potentially affected, resulting in changes in their short-range order, thus directly decreasing lens transparency at the molecular level. Altered vinculin and cadherin could lead to altered cell adhesion, which in turn could modify expected cell-cell signaling. This could have a direct and potentially deleterious impact on fiber-end migration, as seen in the RCS dystrophic rat lenses. The changes in integrin configuration in the RCS lenses could negatively influence mechanotransduction through these receptors, potentially leading to changes in fiber-end migration paths and lenticular pathology. An interactive process that involves rearrangements of vinculin, integrin, and cadherin with a concomitant alteration of F-actin distribution could be responsible for the pathological changes in the RCS rat.

Recent evidence has established that there is an increase in cytokine expression within the retina during retinal degeneration in the RCS rat [26]. Our hypothesis is that these inflammatory cytokines are reaching the lens via the vitreous humor and are potential initiating factors in the aberrant fiber-end migration that characterizes RCS PSCs. As a first step toward exploring this idea, we evaluated whether elevated levels of inflammatory cytokines were present in the vitreous humor before and during the temporal sequence of cataract formation. Inflammatory cytokines, which are multifunctional pleiotypic molecules that elicit their response locally or systemically, were measured using a multiplexed flow cytometry bead-based assay [44-46]. Select inflammatory cytokines, including IL-1 α , IL-4, IL-6, IL-8, TNF, and IFN- γ , were assayed.

IL-1 α is responsible for maturation and proliferation of cells and stimulation of inflammation [44]. In the eye, increased levels of IL-1 have been reported in uveitis and vitreo-retinal disorders [47,48]. In the rabbit eye, it has been

shown that intravitreal IL-1 α stimulated a strong anterior segment inflammation [49]. A similar response has also been documented in Lewis and Fischer rats, which are two different strains [47]. In the present study, increased concentrations of IL-1 α in the vitreous temporally corresponded with the retinal degeneration seen in the RCS dystrophic animals. IL-4 has been shown to play a critical role in cell migration and inflammation in the central nervous system [50]. In the RCS rats, increase in IL-4 levels corresponded with the time of retinal degeneration in these animals similar to that of IL-1 α . In addition to being a potent regulator of the acute inflammatory phase [44,51], IL-6 has also been implicated in increased cell migration in various types of cancers [52,53]. In light of IL-6's role in the migratory process, a sustained uncontrolled production of IL-6, as seen in the dystrophic RCS animals, could have a critical role to play in the abnormal fiber-end migration and the altered cell-cell adhesion seen in the lens. Exogenous IL-8 activity has been documented in the eye and therefore could be responsible for general ocular inflammation as documented in two rodent strains (Lewis and Fischer rats) [47]. The change in cell morphology that is seen in the severely affected lenses at 7-8 weeks of age [21] could be attributed to a possible delayed stimulation of IL-8 levels at this age. Although the present study did not document changes beyond 8 weeks postnatal, the sustained levels of IL-8 at 7-8 weeks of age suggest that it could possibly lead to the mature cataract that is typically seen in the subset of lenses that progress to cortical degeneration in the adult dystrophic RCS rats. TNF has actions on several different tissue types and usually is found to function together with IL-1 and IL-6 [54,55]. Production of TNF, IL-1, and IL-6 is beneficial in response to infection but can be dangerous in inappropriate amounts or with overproduction [55]. TNF has been implicated in causing some of the pathological responses that occur in inflammatory conditions, such as cerebral pathology, arthritis, glomerulonephritis, and other systemic conditions [56-58]. TNF either directly or indirectly is known to activate downstream signaling cascades that influence cell shape, cell migration, formation of filopodia, and cell survival [59,60]. The elevated levels of TNF are seen to temporally correspond with the changes in fiber-end migration observed in the RCS dystrophic animals. It follows, therefore, that TNF could play a critical role in initiating the pathological changes seen in the RCS/Lav lenses.

In the eye, increased levels of IFN have been associated with retinopathy [61] and in a similar fashion could be elevated during the retinal degenerative process in the RCS animals. This cytokine, similar to IL-8, could play an important role in the subset of RCS lenses that do not internalize the PSC but instead proceed to cortical liquefaction.

When analyzing the BMC architecture in the RCS/Lav lenses in light of intravitreal cytokine levels, some striking relationships can be speculated to help explain the changes seen during PSC formation. The integrin family of extracellular matrix receptors regulates various aspects of cell function, in particular cell adhesion and migration [32,62-67]. Integrin binding with cytokines causes recruitment of focal adhesion kinase (FAK) and its phosphorylation [68-70]. Phosphorylated FAK in turn can influence lamellipodia and filopodia formation, loss of intercellular adhesion, cell breakdown, and increased migration [60,71]. Integrin is also known to inactivate Ras homolog gene family, member A (RhoA), which results in the disassembly of focal adhesions [72] seen as the loss of discrete vinculin staining in our model. Integrins are important switch points for the spatiotemporal control of actin-based motility [31,64,66-68,73-75], and a potential loss of controlled interactions between integrins and the downstream mediators could be resulting in the observed structural changes, leading to faulty migration of the fiber ends with consequent changes in suture pattern, cell breakdown, and opacity formation in the RCS rat. In the RCS/Lav rat lenses, three of the characteristic structural alterations, including, altered filopodial configurations, abnormal fiber-end migration, and loss of end-end adhesion/packing, could be due to the altered cadherin distribution. This could explain the initial lack of directionality of the filopodia and the abnormal fiber-end migration [21]. Also, the redistribution of cadherin from its normal basolateral domain to a predominantly basal domain presentation could be responsible for the transient cessation of fiber-end migration seen in these lenses. Rearrangements of vinculin could also result in secondary F-actin rearrangements, which could be compensatory in character/function, stabilizing the fiber ends and preventing further disintegration.

In conclusion, the data strongly indicate the importance of precise fiber-end migration along predetermined paths for the maintenance of lens transparency. A deviation from normal migration paths not only affects the growth shell in which it occurs but also affects succeeding growth shells, thus resulting in not just initiation but also the continued propagation of lenticular pathology (loss of transparency). In summary, this study elucidated the molecular distribution of BMC components during PSC formation in RCS rats. Our data indicate that defined molecular rearrangements precede and characterize the aberrant migration patterns and altered structure of basal fiber ends. The reorganization of BMC architecture is consistent with alterations in adhesion mechanics involving cell-cell attachment, cell-matrix interactions, and timely fiber-end detachment. Our results also suggest that abnormal fiber-end migration could be instigated

by pro-inflammatory cytokines present in the vitreous after the initiation of retinal degeneration.

ACKNOWLEDGMENTS

Portions of this work were presented at the 2009 and 2010 ARVO Annual Meetings. The authors thank Mr. Sean T. Donohue and Ms. Dana K. Williams for their valuable technical assistance. This work was supported by NIH NEI grant R01EY014902 (KJA) and by the Mary Lou Bell McGrew Fund (Rush University), Chicago, IL.

REFERENCES

1. Bassnett S, Missey H, Vucemilo I. Molecular architecture of the lens fiber cell basal membrane complex. *J Cell Sci* 1999; 112:2155-65. [PMID: 10362545].
2. Menko AS, Philip NJ. Beta 1 integrins in epithelial tissues: a unique distribution in the lens. *Exp Cell Res* 1995; 218:516-21. [PMID: 7540985].
3. Menko S, Philp N, Veneziale B, Walker J. Integrins and Development: how might these receptors regulate differentiation of the lens. *Ann N Y Acad Sci* 1998; 842:36-41. [PMID: 9599291].
4. Ireland ME, Braunsteiner A, Mrock L. Cell-cell interactions affect the accumulation of a cytokeratin-like protein during lens fiber development. *Dev Biol* 1993; 160:494-503. [PMID: 7504636].
5. Lovicu FJ, Chamberlain CG, McAvoy JW. Differential effects of aqueous and vitreous on fiber differentiation and extracellular matrix accumulation in lens epithelial explants. *Invest Ophthalmol Vis Sci* 1995; 36:1459-69. [PMID: 7775124].
6. Kurosaka D, Kato K, Oshima T, Kurosaka H, Yoshino M, Ogata M. Extracellular matrix influences proliferation of cultured porcine lens epithelial cells. *Nippon Ganka Gakkai Zasshi* 1999; 103:432-5. [PMID: 10410554].
7. Ferreira-Cornwell MC, Veneziale RW, Grunwald GB, Menko AS. N-cadherin function is required for differentiation-dependent cytoskeletal reorganization in lens cells in vitro. *Exp Cell Res* 2000; 256:237-47. [PMID: 10739670].
8. Traas J, Ramaekers FCS. The membrane-associated cytoskeleton in cultured lens epithelial cells. *Exp Eye Res* 1986; 43:519-28. [PMID: 3539628].
9. Lu J, Kuszak JR, Al-Ghoul KJ. Localization of basal membrane complex components at lens sutures. *ARVO Abs.* 2002; 457:18-.
10. Ramaekers FC, Osborn M, Schmid E, Weber K, Bloemendal H, Franke WW. Identification of the cytoskeletal proteins in lens-forming cells, a special epithelioid cell type. *Exp Cell Res* 1980; 127:309-27. [PMID: 7189714].
11. Ramaekers FCS, Bloemendal H. Cytoskeletal and contractile structures in lens cell differentiation, in *Molecular and cellular biology of the eye lens*, H. Bloemendal, Editor. 1981, John Wiley & Sons: New York. p. 85-136.

12. Rafferty NS, Scholz DL, Goldberg M, Lewycky M. Immunocytochemical evidence for an actin-myosin system in lens epithelial cells. *Exp Eye Res* 1990; 51:591-600. [PMID: 2249732].
13. Wride MA. Cellular and molecular features of lens differentiation: a review of recent advances. *Differentiation* 1996; 61:77-93. [PMID: 8983174].
14. Lee A, Fischer RS, Fowler VM. Stabilization and remodeling of the membrane skeleton during lens fiber cell differentiation and maturation. *Dev Dyn* 2000; 217:257-70. [PMID: 10741420].
15. Fischer RS, Lee A, Fowler VM. Tropomodulin and tropomyosin mediate lens cell actin cytoskeleton reorganization in vitro. *Invest Ophthalmol Vis Sci* 2000; 41:166-74. [PMID: 10634617].
16. Lu JY, Mohammed TA, Donohue ST, Al-Ghoul KJ. Distribution of basal membrane complex components in elongating lens fibers. *Mol Vis* 2008; 14:1187-203. [PMID: 18596883].
17. Al-Ghoul KJ, Kuszak JR, Lu JY, Owens MJ. Morphology and organization of posterior fiber ends during migration. *Mol Vis* 2003; 9:119-28. [PMID: 12707642].
18. Al-Ghoul KJ, Novak LA, Kuszak JR. The structure of posterior subcapsular cataracts (PSCs) in the Royal College of Surgeons (RCS) rats. *Exp Eye Res* 1998; 67:163-77. [PMID: 9733583].
19. Al-Ghoul KJ, Peterson KL, Kuszak JR. The internalization of posterior subcapsular cataracts (PSCs) in Royal College of Surgeons (RCS) rats. I. Morphological characterization. *Mol Vis* 1999; 5:6-[PMID: 10329769].
20. Kuszak JR, Al-Ghoul KJ, Novak LA, Peterosn KL, Herbert KL, Sivak JG. The internalization of posterior subcapsular cataracts (PSCs) in Royal College of Surgeons (RCS) rats. II. The inter-relationship of optical quality and structure as a function of age. *Mol Vis* 1999; 5:7-[PMID: 10329770].
21. Joy A, Mohammed TA, Al-Ghoul KJ. Abnormal fiber end migration in Royal College of Surgeons rats during posterior subcapsular cataract formation. *Mol Vis* 2010; 16:1453-66. [PMID: 20806082].
22. D'Cruz PM, Yasumura D, Weir J, Matthes MT, Abderrahim H, LaVail MM, Vollrath D. Mutation of the receptor tyrosine kinase gene *Mertk* in the retinal dystrophic RCS rat. *Hum Mol Genet* 2000; 9:645-51. [PMID: 10699188].
23. Gal A, Li Y, Thompson DA, Weir J, Orth U, Jacobson SG, Apfelstedt-Sylla E, Vollrath D. Mutations in *MERTK*, the human orthologue of the RCS rat retinal dystrophy gene, cause retinitis pigmentosa. *Nat Genet* 2000; 26:270-1. [PMID: 11062461].
24. Nandrot EF, Dufour EM. *Mertk* in daily retinal phagocytosis: a history in the making. *Adv Exp Med Biol* 2010; 664:133-40. [PMID: 20238011].
25. Lee YJ, Han JY, Byun J, Park HJ, Park EM, Chong YH, Cho MS, Kang JL. Inhibiting *Mer* receptor tyrosine kinase suppresses *STAT1*, *SOCS1/3*, and *NF-kB* activation and enhances inflammatory responses in lipopolysaccharide-induced acute lung injury. *J Leukoc Biol* 2012; 91:921-32. [PMID: 22427680].
26. Liu Y, Yang X, Utheim TP, Guo C, Xiao M, Liu Y, Yin Z, Ma J. Correlation of cytokine levels and microglial cell infiltration during retinal degeneration in RCS rats. *PLoS ONE* 2013; 8:[PMID: 24349184].
27. Al-Ghoul KJ, Lu J. A Terminal Web-Like Structure Is Present In Superficial Cortical Lens Fibers. *Exp Eye Res* 2004; 79:152-.
28. Leong L, Menko AS, Grunwald GB. Differential expression of N- and B-cadherin during lens development. *Invest Ophthalmol Vis Sci* 2000; 41:3503-10. [PMID: 11006245].
29. Menko S. Lens epithelial cell differentiation. *Exp Eye Res* 2002; 75:485-90. [PMID: 12457861].
30. Beebe DC, Vasiliev O, Guo J, Shui YB, Bassnett S. Changes in adhesion complexes define stages in the differentiation of lens fiber cells. *Invest Ophthalmol Vis Sci* 2001; 42:727-34. [PMID: 11222534].
31. Brakebusch C, Fassler R. The integrin-actin connection, an eternal love affair. *EMBO J* 2003; 22:2324-33. [PMID: 12743027].
32. Grose R, Hutter C, Bloch W, Thorey I, Watt FM, Fassler R, Brakebusch C, Werner S. A crucial role of beta 1 integrins for keratinocyte migration in vitro and during cutaneous wound repair. *Development* 2002; 129:2303-15. [PMID: 11959837].
33. Geiger B. Adherin' with cadherin. *Curr Biol* 1991; 1:237-8. [PMID: 15336130].
34. Joy A, Currie MS, Donohue ST, Al-Ghoul KJ. Aberrant basal fiber end migration underlies structural malformations in a streptozotocin-induced diabetic rat model. *Exp Eye Res* 2009; 89:344-57. [PMID: 19358842].
35. Linask KK, Ludwig C, Han MD, Liu X, Radice GL, Knudsen KA. N-cadherin/catenin-mediated morphoregulation of somite formation. *Dev Biol* 1998; 202:85-102. [PMID: 9758705].
36. Wicha MS, Liotta LA, Garbisa S, Kidwell WR. Basement membrane collagen requirements for attachment and growth of mammary epithelium. *Exp Cell Res* 1979; 124:181-90. [PMID: 499382].
37. Terranova VP, Rohrbach DH, Martin GR. Role of laminin in the attachment of PAM 212 (epithelial) cells to basement membrane collagen. *Cell* 1980; 22:719-26. [PMID: 7460011].
38. Sugrue SP, Hay ED. Response of basal epithelial cell surface and Cytoskeleton to solubilized extracellular matrix molecules. *J Cell Biol* 1981; 91:45-54. [PMID: 7197682].
39. Emerman JT, Pitelka DR. Maintenance and induction of morphological differentiation in dissociated mammary epithelium on floating collagen membranes. *In Vitro* 1977; 13:316-28. [PMID: 559643].
40. Gospodarowicz D, Greenburg G, Birdwell CR. Determination of cellular shape by the extracellular matrix and its correlation with the control of cellular growth. *Cancer Res* 1978; 38:4155-71. [PMID: 359133].

41. Zetter BR, Martin GR, Birwell CR, Gospodarowicz D. Role of the high-molecular-weight glycoprotein in cellular morphology, adhesion, and differentiation. *Ann N Y Acad Sci* 1978; 312:299-316. [PMID: 386881].
42. Ben-Ze'ev A, Farmer SR, Penman S. Protein synthesis requires cell-surface contact while nuclear events respond to cell shape in anchorage-dependent fibroblasts. *Cell* 1980; 21:365-72. [PMID: 6157481].
43. Folkman J, Moscona A. Role of cell shape in growth control. *Nature* 1978; 273:345-9. [PMID: 661946].
44. Feghali CA, Wright TM. Cytokines in acute and chronic inflammation. *Front Biosci* 1997; 2:d12-26. [PMID: 9159205].
45. Maini RN, McGrath IT, Russell AS, Dumonde DC. Cell-mediated immunity to micro-organisms in rheumatoid arthritis. *Ann Rheum Dis* 1971; 30:540-1. [PMID: 5112473].
46. Dumonde DC, Maini RN. The clinical significance of mediators of cellular immunity. *Clin Allergy* 1971; 1:123-39. [PMID: 4949099].
47. Ferrick MR, Thurau SR, Oppenheim MH, Herbort CP, Ni M, Zachariae CO, Matsushima K, Chan CC. Ocular inflammation stimulated by intravitreal interleukin-8 and interleukin-1. *Invest Ophthalmol Vis Sci* 1991; 32:1534-9. [PMID: 2016135].
48. de Vos AF, Klaren VN, Kijlstra A. Expression of multiple cytokines and IL-1RA in the uvea and retina during endotoxin-induced uveitis in the rat. *Invest Ophthalmol Vis Sci* 1994; 35:3873-83. [PMID: 7928184].
49. Rosenbaum JT, Samples JR, Hefeneider SH, Howes EL Jr. Ocular inflammatory effects of intravitreal interleukin 1. *Arch Ophthalmol* 1987; 105:1117-20. [PMID: 3498471].
50. Ponomarev ED, Maresz K, Tan Y, Dittel BN. CNS-derived interleukin-4 is essential for the regulation of autoimmune inflammation and induces a state of alternative activation in microglial cells. *J Neurosci* 2007; 27:10714-21. [PMID: 17913905].
51. Heinrich PC, Castell JV, Andus T. Interleukin-6 and the acute phase response. *Biochem J* 1990; 265:621-36. [PMID: 1689567].
52. Walter M, Liang S, Ghosh S, Hornsby PJ, Li R. Interleukin 6 secreted from adipose stromal cells promotes migration and invasion of breast cancer cells. *Oncogene* 2009; 28:2745-55. [PMID: 19483720].
53. Nilsson MB, Langley RR, Fidler IJ. Interleukin-6, secreted by human ovarian carcinoma cells, is a potent proangiogenic cytokine. *Cancer Res* 2005; 65:10794-800. [PMID: 16322225].
54. Beutler B, Greenwald D, Hulmes JD, Chang M, Pan YC, Mathison J, Ulevitch R, Cerami A. Identity of tumour necrosis factor and the macrophage-secreted factor cachectin. *Nature* 1985; 316:552-4. [PMID: 2993897].
55. Gaur U, Aggarwal BB. Regulation of proliferation, survival and apoptosis by members of the TNF superfamily. *Biochem Pharmacol* 2003; 66:1403-8. [PMID: 14555214].
56. Black RL, Oglesby RB, Von Sallmann L, Bunim JJ. Posterior subcapsular cataracts induced by corticosteroids in patients with rheumatoid arthritis. *JAMA* 1960; 174:166-71. [PMID: 13801171].
57. Probert L, Akassoglou K, Alexopoulou L, Douni E, Haralambous S, Hill S, Kassiotis G, Kontoyiannis D, Pasparakis M, Plows D, Kollias G. Dissection of the pathologies induced by transmembrane and wild-type tumor necrosis factor in transgenic mice. *J Leukoc Biol* 1996; 59:518-25. [PMID: 8613699].
58. Bonventre JV, Weinberg JM. Recent advances in the pathophysiology of ischemic acute renal failure. *J Am Soc Nephrol* 2003; 14:2199-210. [PMID: 12874476].
59. Kutsuna H, Suzuki K, Kamata N, Kato T, Hato F, Mizuno K, Kobayashi H, Ishii M, Kitagawa S. Actin reorganization and morphological changes in human neutrophils stimulated by TNF, GM-CSF, and G-CSF: the role of MAP kinases. *Am J Physiol Cell Physiol* 2004; 286:C55-64. [PMID: 12954601].
60. Mattila PK, Lappalainen P. Filopodia: molecular architecture and cellular functions. *Nat Rev Mol Cell Biol* 2008; 9:446-54. [PMID: 18464790].
61. Savant V, Gillow T. Interferon-associated retinopathy. *Eye (Lond)* 2003; 17:534-6. [PMID: 12802361].
62. Hynes RO. Integrins: versatility, modulation, and signaling in cell adhesion. *Cell* 1992; 69:11-25. [PMID: 1555235].
63. Gumbiner BM. Cell adhesion: the molecular basis of tissue architecture and morphogenesis. *Cell* 1996; 84:345-57. [PMID: 8608588].
64. Huttenlocher A, Lakonishok M, Kinder M, Wu S, Truong T, Knudsen KA, Horwitz AF. Integrin and cadherin synergy regulates contact inhibition of migration and motile activity. *J Cell Biol* 1998; 141:515-26. [PMID: 9548728].
65. Horwitz AR, Parsons JT. Cell migration—moving on. *Science* 1999; 286:1102-3. [PMID: 10610524].
66. Schoenwaelder SM, Burridge K. Bidirectional signaling between the cytoskeleton and integrins. *Curr Opin Cell Biol* 1999; 11:274-86. [PMID: 10209151].
67. Holly SP, Larson MK, Parise LV. Multiple roles of integrins in cell motility. *Exp Cell Res* 2000; 261:69-74. [PMID: 11082276].
68. Miyamoto S, Teramoto H, Coso OA, Gutkind JS, Burbelo PD, Akiyama SK, Yamada KM. Integrin function: molecular hierarchies of cytoskeletal and signaling molecules. *J Cell Biol* 1995; 131:791-805. [PMID: 7593197].
69. Miyamoto S, Akiyama SK, Yamada KM. Synergistic roles for receptor occupancy and aggregation in integrin transmembrane function. *Science* 1995; 267:883-5. [PMID: 7846531].
70. Arthur WT, Noren NK, Burridge K. Regulation of Rho family GTPases by cell-cell and cell-matrix adhesion. *Biol Res* 2002; 35:239-46. [PMID: 12415742].
71. Etienne-Manneville S, Hall A. Cdc42 regulates GSK-3beta and adenomatous polyposis coli to control cell polarity. *Nature* 2003; 421:753-6. [PMID: 12610628].

72. DeMali KA, Barlow CA, Burridge K. Recruitment of the Arp2/3 complex to vinculin: coupling membrane protrusion to matrix adhesion. *J Cell Biol* 2002; 159:881-91. [PMID: 12473693].
73. Clark EA, Brugge JS. Integrins and signal transduction pathways: the road taken. *Science* 1995; 268:233-9. [PMID: 7716514].
74. Sheppard D. Epithelial integrins. *Bioessays* 1996; 18:655-60. [PMID: 8760339].
75. Ridley AJ, Schwartz MA, Burridge K, Firtel RA, Ginsberg MH, Borisy G, Parsons JT, Horwitz AR. Cell migration: integrating signals from front to back. *Science* 2003; 302:1704-9. [PMID: 14657486].

Articles are provided courtesy of Emory University and the Zhongshan Ophthalmic Center, Sun Yat-sen University, P.R. China. The print version of this article was created on 31 December 2014. This reflects all typographical corrections and errata to the article through that date. Details of any changes may be found in the online version of the article.